



ELSEVIER

Available online at www.sciencedirect.com**ScienceDirect**journal homepage: www.elsevier.com/locate/bbe**Original Research Article**

Retinal blood vessel segmentation employing image processing and data mining techniques for computerized retinal image analysis



CrossMark

R. GeethaRamani, Lakshmi Balasubramanian*

Department of Information Science and Technology, College of Engineering, Guindy, Anna University,
Chennai, India

ARTICLE INFO**Article history:**

Received 6 February 2015

Received in revised form

17 June 2015

Accepted 24 June 2015

Available online 10 July 2015

Keywords:

Retina

Blood vessels

Gabor filtering

Classification

Clustering

Fundus images

ABSTRACT

Most of the retinal diseases namely retinopathy, occlusion etc., can be identified through changes exhibited in retinal vasculature of fundus images. Thus, segmentation of retinal blood vessels aids in detecting the alterations and hence the disease. Manual segmentation of vessels requires expertise. It is a very tedious and time consuming task as vessels are only a few pixels wide and extend almost throughout entire span of the fundus image. Employing computational approaches for this purpose would help in efficient retinal analysis. The methodology proposed in this work involves sequential application of image pre-processing, supervised and unsupervised learning and image post-processing techniques. Image cropping, color transformation and color channel extraction, contrast enhancement, Gabor filtering and halfwave rectification are sequentially applied during pre-processing stage. A feature vector is formed from the pre-processed images. Principal component analysis is performed on the feature vector. K-means clustering is executed on this outcome to group pixels as either vessel or non-vessel cluster. Out of the two groups, the identified non-vessel group undergoes an ensemble classification process employing root guided decision tree with bagging, while vessel group is left unprocessed as further processing might increase misclassifications of vessels as non-vessels. The resultant segmented image is formed through combining the results of clustering and ensemble classification process. The vessel segmented output from previous phase is post-processed through morphological techniques. The proposed technique is validated on images from publicly available DRIVE database. The proposed methodology achieves an accuracy of 95.36%, which is comparable with the existing blood vessel segmentation techniques.

© 2015 Nałęcz Institute of Biocybernetics and Biomedical Engineering. Published by Elsevier Sp. z o.o. All rights reserved.

* Corresponding author at: Department of Information Science and Technology, College of Engineering, Guindy, Anna University, Chennai, 600025, India.

E-mail addresses: rgeetha@yahoo.com (R. GeethaRamani), lakshmi@auist.net, latchu234@gmail.com (L. Balasubramanian).

<http://dx.doi.org/10.1016/j.bbe.2015.06.004>

0208-5216/© 2015 Nałęcz Institute of Biocybernetics and Biomedical Engineering. Published by Elsevier Sp. z o.o. All rights reserved.

1. Introduction

Fundus imaging [1] provides a valuable resource for analysis of the retina. The fundus image of the retina discloses anatomical structures [2] such as retinal vasculature, optic disk, macula and abnormal structures such as microaneurysms, hemorrhages, exudates, cottonwool spots etc., if present. Optic disk (exposed as a bright oval structure) represents the start of the optic nerve head and is the entry point for major blood vessels to the eye. Macula (observed as a dark region devoid of vessels) with the fovea at its center is responsible for central and high resolution vision. The blood vasculature is a tree like structure spanning across the fundus image. It is a high frequency component exhibited more clearly at high contrast. The retinal blood vessels are one of the most important structures of the retina providing blood supply to the retina and also transmitting the information signals from the retina to the brain [3].

The changes in retinal blood vessels serve as a bio-marker for identification of many disorders such as diabetic retinopathy, hypertensive retinopathy, retinal artery occlusion, retinal vein occlusion, etc. Not only retinal diseases, but also diseases such as stroke, hypertension and diabetes produce noticeable alterations in the retinal blood vasculature. Most of the retinal disorders that cause modifications in the vascular network would lead to vision loss. Diagnosing these disorders, at the initial stage can prevent the vision loss to a greater extent. Changes in the vascular network pertain to its shape, width, tortuosity, branching pattern etc. Hence segmentation of blood vessels in the fundus image and further analysis of its properties aids in diagnosis of retinal vascular disorders. Also, segmentation of blood vessels and hence extraction of vascular points is useful for image registration [3]. Even for people with expertise, segmentation of blood vessels is a time consuming and effort prone process. Utilization of the power of computational intelligence to automatically segment the blood vessels in fundus images would be highly appreciated by the ophthalmologists. Various such techniques have been adopted in the literature to segment the retinal vessels. However, automatic segmentation of retinal blood vessels is also challenging due to the various complications pertaining to its structure and influence from other sources. The difficulties arise due to variations in vessel appearance, shape and orientations; low contrast between the blood vessels and its background; disturbances caused to the presence of noise and the existence of abnormal structures such as lesions, exudates, microaneurysms and other diseased regions. These complications might mislead an automatic vessel segmentation algorithm by misinterpreting background to vessels and overlooking or missing the thin vessels.

In this research, a blood vessel segmentation approach for segmenting the blood vessels in fundus images is presented. This approach attempts to segment the vessels through chronological application of image pre-processing (image cropping, color transformation and color extraction, Gabor filtering, halfwave rectification), supervised and unsupervised learning (principal component analysis, clustering and classification) and image post-processing techniques. The review of the state-of-art techniques in retinal blood vessel segmentation, the

dataset used for validation, the methodology proposed, experimental results of the work and the conclusions are presented in detail in the further sections.

2. Review of the related studies

Retinal blood vessel segmentation is achieved through assigning each pixel as either a vessel pixel or non-vessel pixel. The retinal vessel segmentation methodologies can be seen in different dimensions. In a broad sense, the vessel segmentation methodologies can be divided into two categories namely rule based techniques and pattern recognition based techniques. Vessel tracking, matched filtering, mathematical morphology, multi-scale techniques and model based approaches fall under the rule based category [4]. Alternatively, supervised techniques involving building classification models for categorization of the pixels and clustering models for grouping of pixels as either vessel or non-vessel pixels are included under the pattern recognition based techniques. The supervised methodologies require data of manually labeled vessel and non-vessel pixels for the purpose of training the model which is used for classification.

Regarding the pattern recognition based methodologies; generally there exist two stages where during the first stage, image is enhanced and required features are extracted followed by the second stage which classifies each pixel as either a vessel or non-vessel. A few attempts to classify the pixels were made through the supervised techniques which are concisely highlighted here. These methods differ in the feature vector and classification process adopted. Since blood vessels are elongated structures in the fundus image, Staal et al. [5] utilized the concept of ridges for vessel extraction. The properties of the ridges and the pixel considered forms the feature vector. K-nearest neighbor (KNN) classification procedure, which gave better results than a linear and quadratic classifier was adopted for classifying the image ridges achieving an accuracy of 94.41% with a computational time of 900 s using 1 GHz processor. Subsequently, Niemeijer et al. [6] attempted KNN classification on a 31D feature vector which included the intensity of green channel and responses of Gaussian and its derivative at various scales resulting in an accuracy of 94.16%. Then, Soares et al. [7] utilized Bayesian classifier with Gaussian mixture models for fast classification on a feature vector comprising of Gabor wavelet responses at various scales, providing an accuracy of 94.66%. This methodology used one million pixels for training and consumed 9 h for training and 30 s for classification. In another attempt, Marin et al. [8] demonstrated a neural network based classifier (non-linear classification procedure) on a 7D feature vector formed from the gray level and the moment invariant features achieving an accuracy of 94.52%. This method processes an image in less than 90 s due to its simplicity of operation. Again, Franklin et al. [3] made an attempt using neural networks to segment retinal vessels, through a feature vector formed using the intensities of red, green and blue channels of the RGB image yielding an accuracy of 95.03%.

Strategies were introduced to deal with large and small vessels separately. Xu et al. [9] adopted Adaptive local thresholding to extract large vessels and support vector

machines (SVM) for classification of thin vessels in the residual image, represented by a 12D vector, resulting in an accuracy of 93.20%. Then, You et al. [10] proposed another integration based technique in which radial projection was employed for extraction of thin vessels and SVM was used to classify the major vessels using the feature vector formed from the wavelet co-efficients at different scales, accomplishing an accuracy of 94.34%. These integration approaches [9,10] yielded higher sensitivity but resulted in lower overall accuracy. In general, algorithms that learn from training images report better segmentation accuracies at the cost of higher computational times. Since the retinal vascular structure is complex and exhibits a high level of variability, enhancements and simple thresholding cannot yield impressive performance. Sophisticated decision making process adopted by supervised learning methods can help to overcome this issue.

Rule based techniques were also adopted for the purpose of retinal blood vessel segmentation. Firstly a few works on matched filtering is presented here. The matched filtering (MF) approach convolves a 2D kernel with the retinal fundus image such that the matched filter response (MFR) indicates the presence or absence of vessels. Since blood vessels are piecewise linear in structure, the blood vessels could be better captured through appropriately designed filters. Chaudhuri et al. [11] put forward a 2D linear kernel with Gaussian profile, which on rotating every 15° extracted the blood vessels in different orientation reaching an accuracy of 87.75%. Then, Kande et al. [12] came up with a spatially weighted fuzzy C means clustering that accommodates the spatial distribution of gray levels to threshold the MFR, owing to complex relationships between foreground and background by them, resulting in an accuracy of 89.11%. Subsequently, a knowledge guided adaptive thresholding that takes advantage of domain knowledge about the blood vessels was investigated for vessel extraction by Xiaoyi and Mojon [13] achieving an accuracy of 92.12%. After that, Cinsdikici and Aydin [14] introduced a hybrid approach which employs MF and ant colony clustering on fundus image in parallel, to improve the performance of vessel segmentation, followed by application of length filtering, exhibiting an accuracy of 92.93%. To take advantage of the fact that Gaussian shape profile is symmetric about its peak, Zhang et al. [15] computed the first order derivatives and hence could eliminate most of the non-vessel edges thus reducing false detections and resulting in an accuracy of 93.82%. Vesselness filter proposed by Frangi [16] uses eigenvectors of the Hessian to compute the likeliness of an image region to contain vessels. Budai et al. [17] performed multi-resolution analysis to decrease the computational complexity. To the reduced resolutions of copies of images, Frangi's vesselness filter was applied. The sensitivity of the system was 64.40%, which was very low when compared to the existing methods. Then, Hannink et al. [18] proposed to use multi-scale orientation scoring followed by application of vesselness filter and tested it on HRF image data. This methodology could handle the vessel crossings and bifurcations as against the vesselness filter which looked only for elongated structures. Then, Chakraborti [19] introduced a self-adaptive MF which is a synergistic combination of vesselness and matched filter yielding an accuracy of 93.70%. In a broad

spectrum, these filter based approaches are based on intensity of the image and are susceptible to intensity inhomogeneity. They face issues while enhancing vessels of different scales. They have to be combined with some other technique to increase the performance of the segmentation algorithms.

The principle of morphological operations has also been extensively used for extraction of retinal blood vessels. A few works in this view are briefed here. Mendonca and Campilho [20] proposed a framework exploiting the properties such as linearity, connectivity and width of blood vessel structure. The methodology includes centerline detection through difference of offset Gaussian filters, vessel enhancement through modified top-hat transform with a circular structural element and segmentation of vasculature using iterative region growing attaining an accuracy of 94.63%. Miri and Mahloojifar [21] investigated a combination of discrete curvelet transform, multi-structural mathematical morphology and adaptive connected component analysis in regard to segmentation of retinal vessels. The effectiveness of curvelet transform in representing edges, the directionality of multi-structure elements in morphology and connected component analysis along with thresholding when combined together could attain an accuracy of 94.58%. Then, Fraz et al. [22] introduced a hybrid procedure combining the vessel centerline extraction and morphological bit slicing reaching an accuracy of 94.30%. Subsequently, isotropic undecimated wavelet transform (IUWT), a popularly used wavelet transform in Biological applications was demonstrated for vessel segmentation by Bankhead et al. [23]. It was observed that the vessels were clearly visible at higher wavelet levels of the transform. This approach comprising of IUWT, thresholding, mathematical morphology and sphline filtering reported an accuracy of 93.71%. After that, Akram et al. [24] utilized Gabor wavelet owing to their capability of capturing directional structures, for enhancing the vessels and adopted multilayer thresholding for vessel segmentation, reaching an accuracy of 94.69%. The methodology is claimed to work well in non-uniform illumination conditions also and captured many thin vessels. Usually, morphological operations consider the connectivity of the neighbors and helps in increasing the performance of segmentation algorithms. These operations appear to be more impressive when performed in combination with the other operations preferably as a post-processing step.

Employing multi-scale approaches for segmentation of retinal blood vessels have become very common in recent times as the variability in width of retinal structures cannot be captured by a single scale parameter. A few works through this method have been narrated here. Martinez-Perez [25] presented a technique based on multi-scale operators to beat the issue of contrast variations by utilizing the first and second spatial derivatives of the intensity image that provides the vessel topology information. Then, local maxima over scales of magnitude of gradient and maximum principal curvature of Hessian Tensor are adopted in multi pass-region growing. It operates on two stages where during the first stage, the growth is constrained to regions of low gradient magnitude together with spatial information about the 8 neighboring pixels and in next stage, the constraint is relaxed to allow boundaries between regions to be defined, achieving an accuracy of 91.81%. An extension of this work by same author [26] included

a diameter dependent equalization factor to multi scale analysis to enhance the sensitivity and accuracy of the approach, thus attaining an accuracy of 93.44%. Then, Anzalone et al. [27] proposed to adopt supervised techniques to choose optimal parameters (scale and threshold) for the purpose of vessel segmentation. It involves vessel enhancement through scale space analysis followed by image binarization through thresholding and could achieve an accuracy of 94.19%. Subsequently, Vlachos and Dermatas [28] presented a technique which yielded high sensitivity measure. Initially line tracking procedure was performed, which initiated from a small group of pixels gained through the brightness selection rule and ceased when a cross-sectional profile becomes invalid. This was done for various scales and combined using the confidence of a pixel belonging to vessel or non-vessel. Then, median filtering and morphological reconstruction was applied to the formed vessel network reporting an accuracy and sensitivity of 92.90% and 74.70%. After that, Saffarzadeh et al. [29] proposed a method based on the idea that elimination of bright lesions could result in higher performance of vessel segmentation. Perspective transformation and K-means clustering was performed to remove the bright lesions. Then, multi-scale line operator was adopted to detect blood vessels, thus achieving an accuracy of 93.87%. Multi-scale approaches helps in identifying vessels with varying width. But, their effectiveness can be exploited only when used as a pre-processing step for vessel enhancement.

Vessel tracking methodologies were also exploited for vessel segmentation, few of which are reported here. Zhou et al. [30] suggested a procedure that adopts MF and is initiated by the start and end point followed by automatic detection of retinal vessels, thus has the inherent disadvantage of user intervention. Then, to overcome this disadvantage, Can et al. [31] presented a procedure which automatically finds the seed point of tracing represented as local gray level minima. The next vessel point is identified through series of exploratory searches which arrives at the vessel boundaries. Then, Tolias and Panas [32] introduced unsupervised fuzzy vessel tracking algorithm which performs automatic initialization and tracks vessels and the categorization of vessel and non-vessel regions are obtained using a fuzzy C-means clustering algorithm. This method also does not demand for initialization and vessel profile modeling.

Model based approaches have also been utilized in the intention of retinal vessel segmentation. These model based methods appear difficult to formulate. A few of them are briefed here. A methodology was demonstrated by Lam et al. [33], which is based on regularization based multi-concavity modeling containing three concavity measures viz., differential, line shape and locally normalized concavity for addressing the negative impact due to bright lesions, dark lesions and noise respectively. The features got from these measures are combined according to the geometrical and statistical properties followed by a lifting procedure to arrive at the ideal vessel shape depicting an accuracy of 94.72%. Then, Espona et al. [34] made use of the combination of concept of snake and the topological properties of vessel for retinal vessel extraction reaching an accuracy of 93.52%.

The extensive research on retinal vessel segmentation presented in this section justifies the need and importance of

the current work. Though a lot of research has been done in this area, there still exists demand for segmentation techniques which achieve higher accuracies. It is to be observed that the previous works projected have attempted to enhance the accuracy of segmentation and an improvement of even 0.03% in accuracy [21,24] was considered significant (since the accuracy levels expected by the field of ophthalmology in detecting blood vessels tend to 100%). Additionally, it can be seen that the approaches used in the literature do not achieve high performance when performed individually. But, each methodology has its own advantage and significance which can be exploited. Filtering enhances the vessels; multi-scale approaches help in capturing the vessels with varying width; supervised and supervised groups predicts the vessels and non-vessels if an efficient feature vector is provided and morphological approaches helps in establishing the connectivity of the pixels. The advantages of these approaches are exploited in our methodology. The data used for validation of the proposed work and the proposed methodology is explained in detail in the subsequent section.

3. Materials and methods

This research work presents a technique for automatically segmenting retinal blood vessels from the fundus image for retinal analysis and disease diagnosis. The changes in the properties of the blood vessels act as a bio-marker for diagnosing many diseases. The retinal vasculature segmentation is a challenging task as the blood vessels are only a few pixels wide and vary in the diameter and also span throughout the fundus. This work constitutes of three phases viz., image pre-processing, supervised and unsupervised learning and image post-processing. The material used for testing the proposed methodology is presented in the following subsection.

3.1. Materials

The data used for validation of the proposed approach is obtained from the publicly available DRIVE database [6,35]. The DRIVE database consists of 40 color fundus images grouped into two sets: test and training each contain 20 images with a resolution of 584×565 pixels. The images were acquired using a Canon CR5 non-mydriatic 3CCD camera with a 45° field of view. Each image was captured using 8 bits per color plane. For each image, a mask image is provided that delineates the field of view. For the training set of images, a single manual segmentation of the blood vessels is available. For the test set of images, two manual segmentations are available out of which, one is used as principal standard, the other one can be used to compare computer generated segmentations with those of an independent human observer. Out of 40 images, 33 are images without any symptoms of pathology and 7 show signs of diabetic retinopathy. Among the 7 images, 3 are available in the training set and 4 are present in the test set. All the 40 images were used for making clinical diagnosis. This database has been extensively used for validation of retinal blood vessel segmentation techniques in the literature. Hence we have also tested and validated our work on the DRIVE

database for comparison purposes. A few example fundus retinal images (left and right eye images) are shown in Fig. 1. Outcomes of each component in the proposed framework will be illustrated on these two images in the further sections.

3.2. Methodology

This research identifies a solution to the retinal blood vessel segmentation problem. The proposed framework is depicted in Fig. 2. This work attempts to segment the blood vessels through 3 stages viz. image-pre-processing, supervised and unsupervised learning and image post-processing. The image pre-processing phase comprises of image cropping, color space transformation and color channel extraction, contrast enhancement, Gabor filtering and halfwave rectification. The output from the image pre-processing stage is given to the supervised and unsupervised learning phase which includes feature vector formation, application of principal component analysis, clustering followed ensemble classification. During the supervised and unsupervised learning phase, the vessel segmentation problem is viewed as a categorization problem. An image pixel should either belong to a vessel pixel or a non-vessel pixel.

The processes adopted during each phase are explained in detail in the following sub sections.

3.2.1. Image pre-processing

Initially, the color fundus image is preprocessed for enhancing the quality of the image and hence to make computation easy and effective. Pre-processing of the fundus image includes image cropping, color space transformation and color channel extraction, contrast enhancement, Gabor filtering and half-wave rectification.

3.2.1.1. Image cropping. The images are cropped such that only the field of view is considered for further investigation. This procedure eliminates the area that is beyond the region of interest. To execute the process of image cropping, a mask that delineates the field of view is formed. The four extreme coordinates (first pixel occupied by the field of view while

traversing from top, left, right and bottom) are attained with the help of this mask. With these co-ordinates, the image is cropped to desired width and height dynamically. This step discards approximately 40,000 pixels (around 50 pixels widthwise and 30 pixels height wise) (around 12% of the total pixels) on DRIVE retinal images having a resolution of 584×565 pixels. The value changes for each image according to the size of field of view. This method thus reduces the size of the image and hence lesser number of pixels is investigated in further computation, reducing the computational complexity. The cropped images are shown in Fig. 3. Image cropping is followed by color transformation.

3.2.1.2. Color space transformation and color channel extraction. The cropped fundus images originally belong to RGB color space which consists of red, green and blue components, out of which the vessels are prominently visible only in the green channel. The task of vessel segmentation could not be performed efficiently with the Gabor responses from Green channel alone. A few other color components which exposed the vessels clearly, were sought for its efficient segmentation. Moreover, RGB color model is not perceptually uniform and Euclidean distances in 3D RGB space do not correspond to color differences as perceived by humans. Hence perceptually uniform color spaces were also exploited to extract the Gabor features. These color spaces are also very efficient in color texture analysis. L*a*b, Gaussian and YCbCr color models were utilized for this purpose. The YCbCr model consists of Y (the luma component), Cb (the chroma of the blue difference) and the Cr (the chroma of the red difference) components and can be derived from the RGB model [36] according to the following equation (Eq. (1)).

$$\begin{bmatrix} Y \\ Cb \\ Cr \end{bmatrix} = \begin{bmatrix} 16 \\ 128 \\ 128 \end{bmatrix} + \begin{bmatrix} 0.257 & 0.504 & 0.098 \\ -0.148 & -0.291 & 0.439 \\ 0.439 & -0.368 & -0.071 \end{bmatrix} * \begin{bmatrix} R \\ G \\ B \end{bmatrix} \quad (1)$$

Again, the RGB color space is converted into L*a*b color space [36], which includes the L (lightness), a and b (color opponent) components according to the algorithm and parameters of Matlab. Also, the RGB color model is converted into the

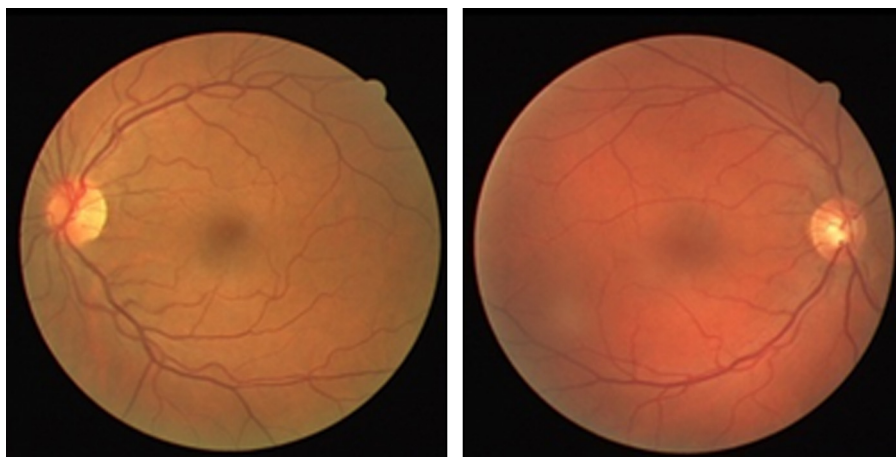


Fig. 1 – Sample retinal images (left and right eye respectively), given as input to the proposed Framework from the DRIVE database.

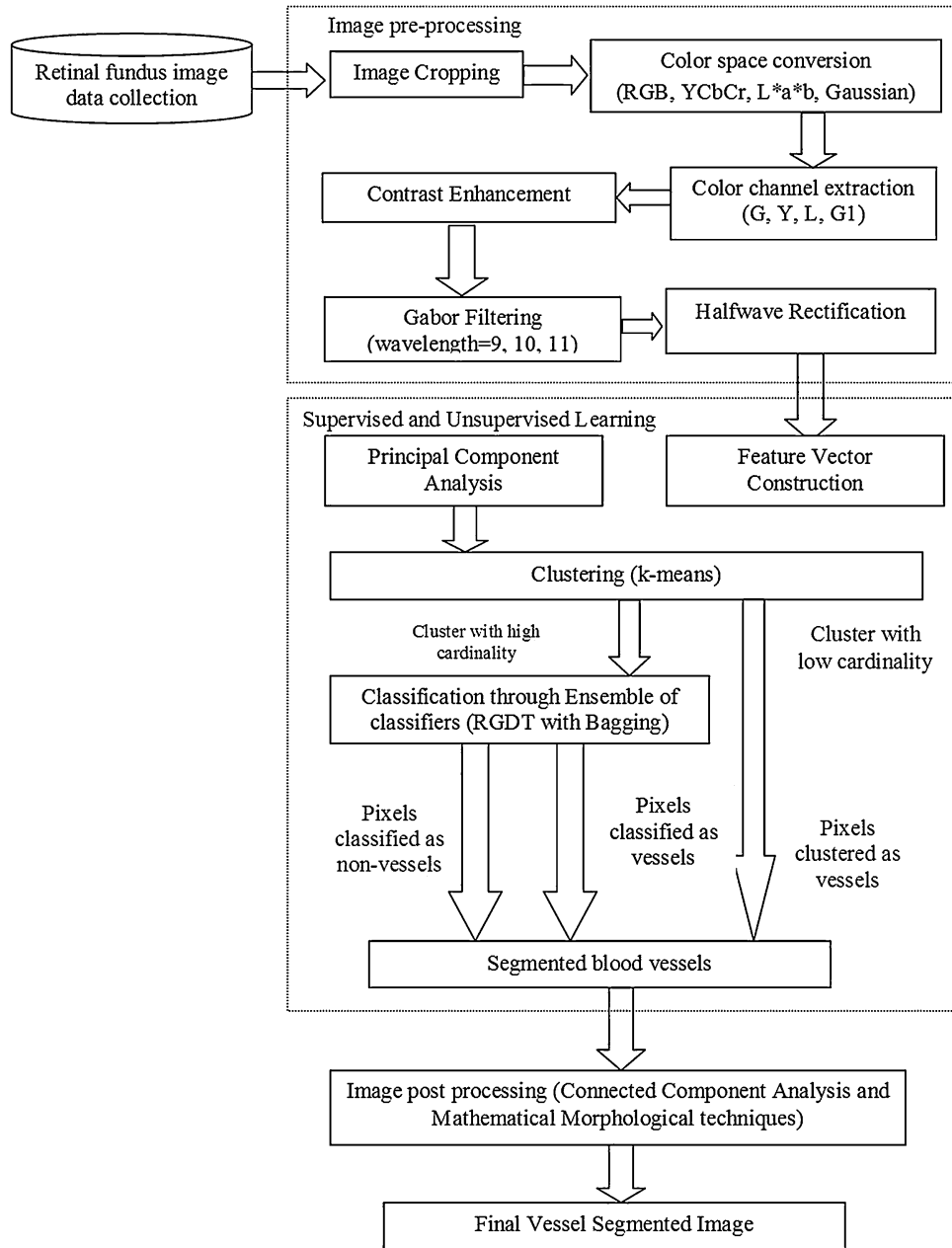


Fig. 2 – Proposed framework for retinal blood vessel segmentation.

Gaussian color space [37], which consists of G1, G2 and G3 components, according to the following transformation equation (Eq. (2)).

$$\begin{bmatrix} G1 \\ G2 \\ G3 \end{bmatrix} = \begin{bmatrix} 0.06 & 0.63 & 0.27 \\ 0.3 & 0.04 & -0.35 \\ 0.34 & -0.6 & 0.17 \end{bmatrix} \begin{bmatrix} R \\ G \\ B \end{bmatrix} \quad (2)$$

Blood vessels are high frequency component of the image and hence are well exposed at high contrast. The four color spaces that were obtained in the earlier step are analyzed and the color channel which exhibited the highest contrast in each color

space was selected for further investigation. In view of this, Green channel from RGB color space, Y channel from YCbCr color space, L channel from L*a*b color space and G1 channel from the Gaussian color space were chosen for further processing. Illustration of these channels can be seen in Fig. 4. The contrast of these images is further improved through the contrast enhancement procedure discussed in the next sub section.

3.2.1.3. Contrast enhancement. The quality of the four color channel images G, Y, L and G1 are elevated through enhancing its contrast. The contrast limited adaptive histogram equalization (CLAHE) [38] is applied to increase the contrast

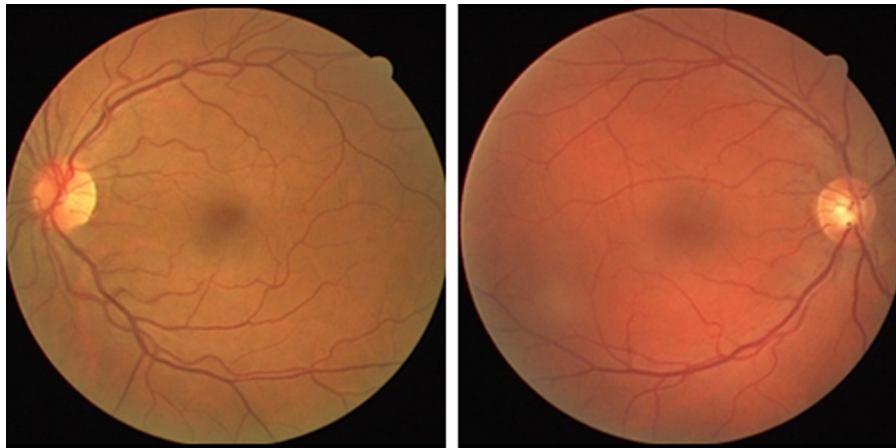


Fig. 3 – Sample images (shown in Fig. 1) after image cropping.

and hence the blood vessels appear more distinguished from the background. The CLAHE operates on small image regions called tiles rather than the whole image. The working of CLAHE algorithm is presented in *Procedure 1*.

The CLAHE algorithm works on image tiles. The clip limit and number of tiles parameters were analyzed to find that the above set value provides better results. The parameter values correspond to the default values of Matlab software.

Step 1: The initial parameter values are set as follows

$$\text{num_of_tiles} = [M \ N] = [8 \ 8]$$

$$\text{num_bins} = 256$$

$$\text{clip_limit} = 0.01$$

Distribution: Uniform

$$\text{Alpha} = 0.4$$

Step 2: Split the image into tiles. Pad the image if needed. (If rows and columns are not a multiple of 8 in this case)

Step 3: Compute the actual clip limit as follows

$$\text{num_of_pixels_in_tile} = M * N \ (64 \text{ in this case})$$

$$\text{min_clip_limit} = \frac{\text{num_of_pixels_in_tile}}{\text{num_bins}}$$

$$\text{actual_clip_limit} = \text{min_clip_limit} + \text{round}(\text{clip_limit} * (\text{num_of_pixel_in_tile} - \text{min_clip_limit}))$$

Step 4: Each tile is processed as follows to produce the corresponding grey level mapping:

Step 4a: Extract a tile and construct its histogram

Step 4b: Clip the histogram using the computed *actual_clip_limit*.

Step 4c: A mapping transformation function for the tile is formulated as follows:

$$\text{sum_of_hist} = \text{cumulative sum}(\text{image_histogram})$$

$$\text{Range} = \max(\text{tile}) - \min(\text{tile})$$

$$\text{scale} = \frac{\text{Range}}{\text{num_of_pixels_in_tile}}$$

$$\text{Mapping} = \min(\min(\text{tile}) + \text{sum_of_hist} * \text{scale}, \max(\text{tile}))$$

Step 5: The final contrast enhanced image is formed through interpolation of grey level mappings as follows.

Step 5a: For each pixel find the four closest neighboring tiles that surround that pixel.

Step 5b: With the pixel intensity as an index, find its mapping at the four neighboring tiles.

Step 5c: Apply bilinear interpolation among these values to obtain the mapping of the currently considered pixel.

Step 5d: This pixel value forms the pixel intensity of the output contrast enhanced image.

Procedure 1: Working of CLAHE algorithm.

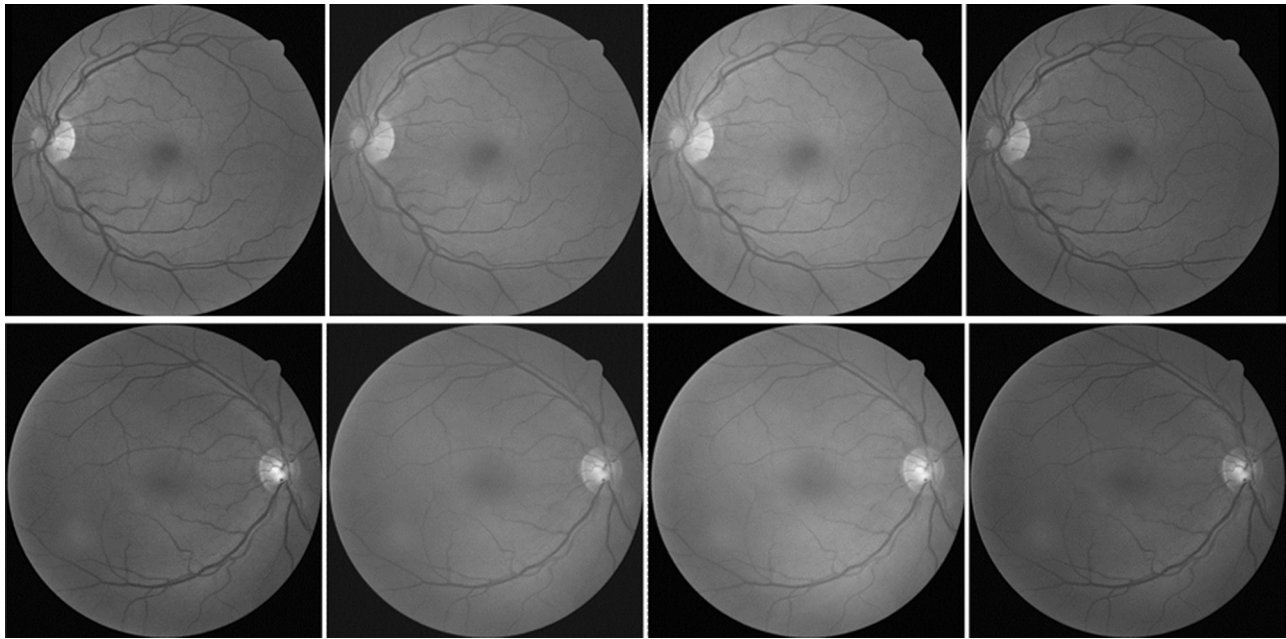


Fig. 4 – Illustrations of green, Y, L and G1 channels of first (left eye image) and second (right eye Image) sample images shown in Fig. 1, portraying high contrast.

When higher values were set to clip limit and number of tiles, the contrast of the background pixels increased, but exposed the non-uniform texture of the background. With lower values for these parameters, the contrast of the vessels was not enhanced to extract them efficiently in the subsequent steps. The size of the tiles is based on the application under consideration. The contrast enhanced images are portrayed in Fig. 5. In continuation to this, Gabor filtering is applied to these four contrast enhanced images, process of which is presented in the next sub section.

3.2.1.4. Gabor filtering. The four contrast enhanced images are considered for further analysis. The blood vessels take the shape of Gaussian approximation. Hence Gaussian based filters can aid in distinguishing the blood vessels of the retinal image. Two dimensional Gabor filters [39], which are sinusoidally modulated Gaussian functions, have been used to enhance the retinal blood vessels. These filters have optimal localization in both frequency and space domains. The performance of the Gabor filters is affected by its parameters to a great extent. Correct choice of the parameter values would result in better

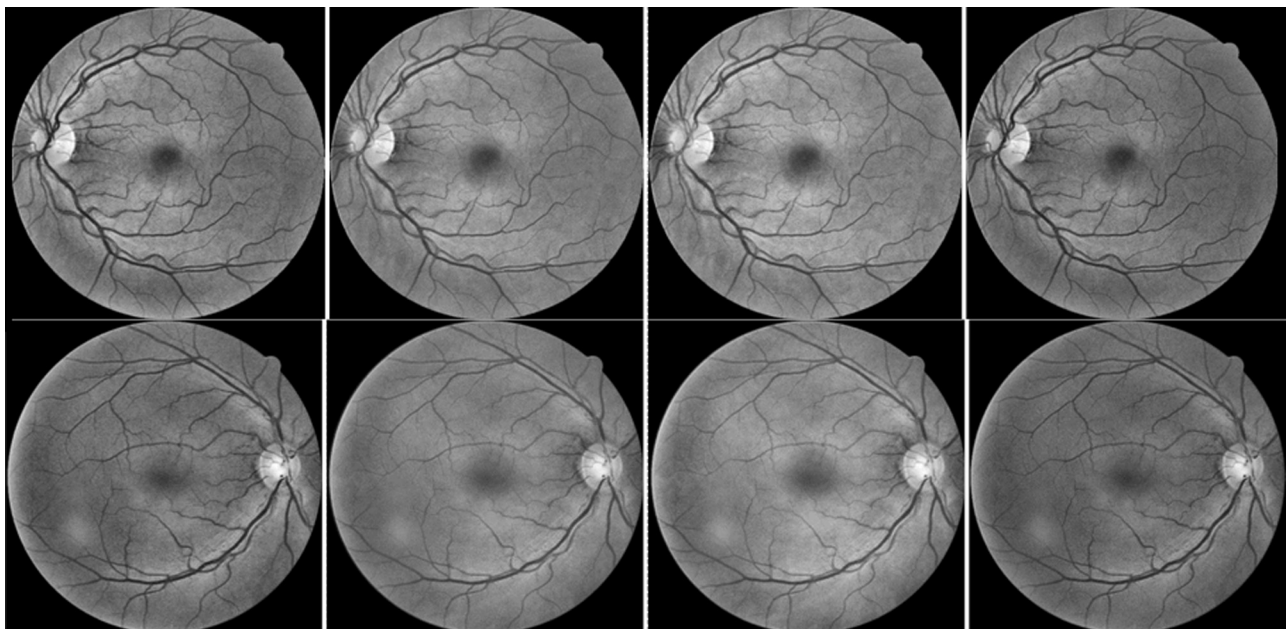


Fig. 5 – First (left eye image) and second (right eye image) sample images after contrast enhancement.

performance of these filters. Gabor filters work on the retinal images as stated in *Procedure 2*.

Step 1: Initialize the filter parameters

wavelength = 9,10,11; *orientation* = 0 degree;
phase offset = [-pi pi]; *aspectratio* = 0.5; *bandwidth* = 1;
NumberOfOrientation = 24;

Step 2: Calculate *sigma* as follows:

$$slratio = \frac{1}{\pi} \sqrt{\frac{\ln(2)}{2} * \frac{2^{bandwidth} + 1}{2^{bandwidth} - 1}}$$

$$\sigma = slratio * wavelength$$

Step 3: Compute the size of 2D Gabor filter kernel as below.

$$n = 2.5 * \frac{\sigma}{aspectratio}$$

Convert the computed value to the lowest whole number.

Size of the kernel matrix = $2n + 1$

Step 4: Construct a mask grid $[x y] = meshgrid(-n:n)$.

Change the direction of $y:y = -y$

Step 5: Construction of 2D Gabor filter kernel is done as follows.

$$f = \frac{2\pi}{wavelength} b = \frac{1}{2*\sigma^2} a = \frac{b}{\pi}$$

$$xp = x \cos \theta + y \sin \theta \quad yp = -x \sin \theta + y \cos \theta \quad cosfunc = \cos((f * xp) - \pi)$$

$$result = a * e^{(-b * (xp^2 + (aspectratio^2 * yp^2)))} * cosfunc$$

Step 6: The positive and negative values are normalized to ensure that the integral of Gabor kernel is 0.

$$pos = sum(positive values in kernel)$$

$$neg = abs(sum(negative values in kernel))$$

Divide every positive and negative value in the kernel with *pos* and *neg* respectively.

Step 7: Convolve the image with the filter kernel

Step 8: Step 2 to Step 7 is repeated for NumberofOrientation= 1 to 24. The peak response from every iteration is accumulated and the final Gabor response image is constructed.

Step 9: Step 2 to 8 is repeated for wavelength=9, 10 and 11.

Procedure 2: Working of Gabor filters on retinal images.

The parameters wavelength, aspect ratio and bandwidth influence the size of Gabor kernel constructed. The size of Gabor kernel should be such that the vessels with varying width are captured. From our experiments, it was observed that the performance of Gabor filtering in capturing the vessel information was highest at wavelength 9, 10 and 11; aspect ratio 0.5 and bandwidth set to one. The retinal vessels are present in all orientations and hence captured by varying the orientation of the filters. Orientation of the filters was initially set to zero and Gabor responses were accumulated for every 15° change until 360° (hence incremented 24 times). The 15° change is acceptable due to the responsiveness of filters for 7.5° in either direction. These Gabor responses form an efficient

feature vector for blood vessel segmentation in the subsequent steps.

Gabor filtering is operated on four contrast enhanced images yielding 12 Gabor response images. These 12 images are halfwave rectified as explained in the next sub-section.

3.2.1.5. Halfwave rectification. Halfwave rectification is applied on the 12 Gabor images. This procedure works on the image based on a percentage value of the maximum intensity of the image. The percentage value was set to 10 in this work. All pixels having a Gabor response value below the percentage will be set to 0. The process of halfwave rectification is illustrated in *Procedure 3*.

Step 1: Find maximum intensity of the image I

$$maxIntensity = \max(I)$$

Step 2: Calculate the percentage value

$$perVal = maxIntensity * \frac{hwpercent}{100}$$

Step 3: Update the values in Matrix I.

$$I = \begin{cases} 0 & I < perVal \\ I & I \geq perVal \end{cases}$$

Procedure 3: Process of halfwave rectification.

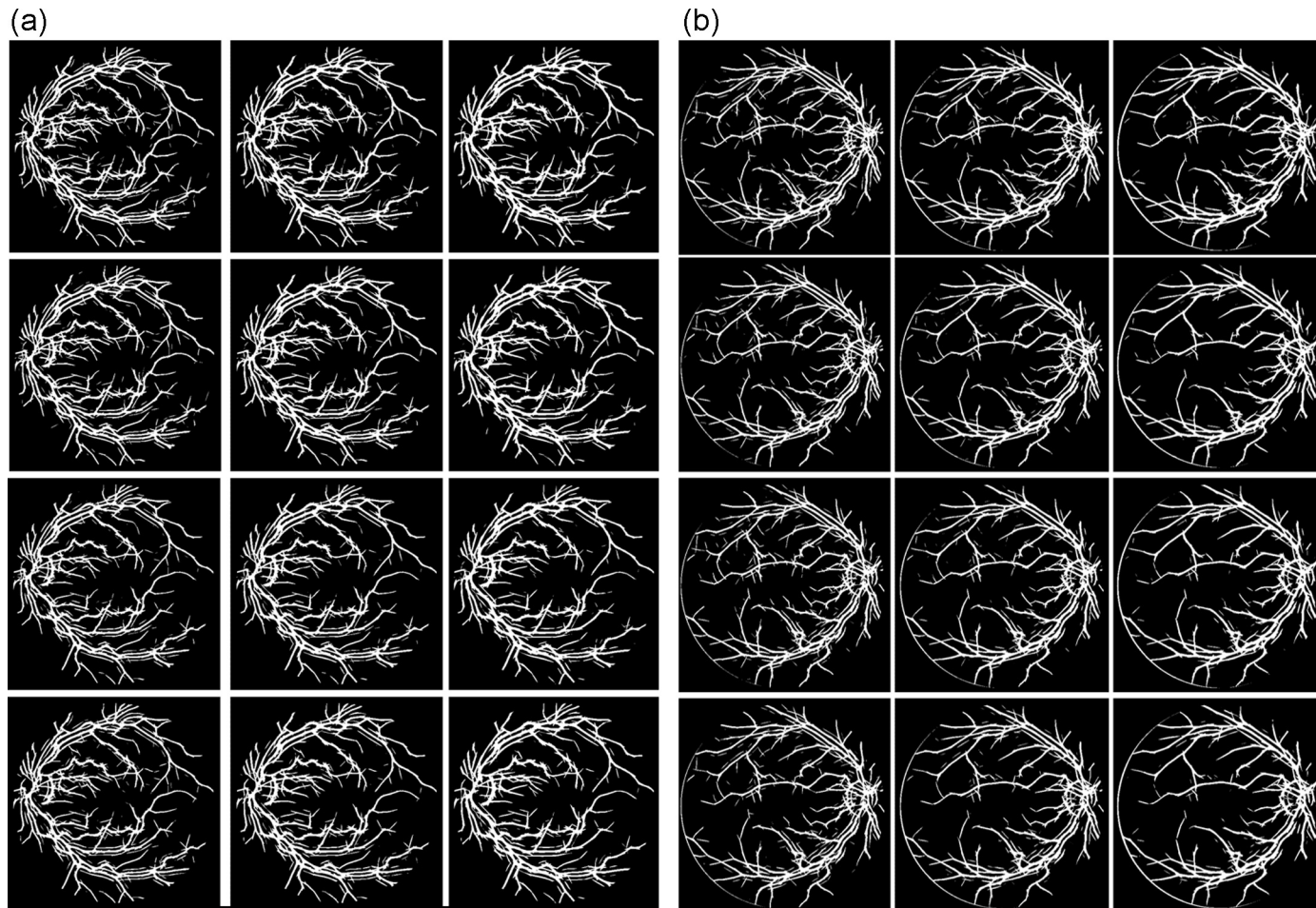


Fig. 6 – (a) Halfwave rectified Gabor response of the green channel at wavelength 9, 10, 11; Y channel at wavelength 9, 10, 11; L channel at wavelength 9, 10, 11; G1 channel at wavelength 9, 10, 11 of the first image (left eye image). (b) Halfwave rectified Gabor response of the green channel at wavelength 9, 10, 11; Y channel at wavelength 9, 10, 11; L channel at wavelength 9, 10, 11; G1 channel at wavelength 9, 10, 11 of the second sample image (right eye image).

The halfwave rectified Gabor images of the two sample images are depicted in Fig. 6(a) and (b). The 12 images appear similar when viewed as a figure, but the Halfwave rectified Gabor responses differ in value. When the wavelength is set to 11, a few thin vessels do not appear while at wavelengths 9, 10, extra false vessel-like structures appear. So the three halfwave rectified Gabor responses of the four color channels are considered for further analysis.

3.2.2.2. Principal component analysis. Principal component analysis [40] has always been a commanding tool in analyzing patterns in high dimensional data. Principal component analysis is applied to the 13 dimensional feature vector to arrive at a new set of more representative 13 dimensional features represented as Eigen vectors. This procedure works on the feature vector in accordance with the algorithm shown in Procedure 4.

- Step 1: Calculate mean of every attribute.
- Step 2: Subtract attribute's mean from each of the data in the attribute
- Step 3: Calculate the covariance matrix (13*13 matrix)
- Step 4: Calculate Eigen vectors and Eigen values for the covariance matrix.
- Step 5: Transpose the Eigen vector and multiply it on left of the transposed original data

Procedure 4: Procedure for application of principal component analysis.

The output of the image pre-processing phase is given as input to the unsupervised and supervised learning phase which is described in detail in the following section.

3.2.2. Unsupervised (principal component analysis and clustering) and supervised learning (ensemble classification) phase
The image data is further analyzed for blood vessel segmentation through supervised and unsupervised data mining techniques. The processes included in the phase are the feature vector formulation, application of principal component analysis, clustering and ensemble classification. These processes are described in detail below.

3.2.2.1. Feature vector formulation. The 12 images from the halfwave rectification step and the green channel from the contrast enhancement step are taken for further consideration. A feature vector is formed such that each pixel in the image is represented by these 13 values which include the intensity in the green channel and the halfwave rectified Gabor responses for that pixel in the 12 images. Hence a 13 dimensional feature vector is formed for further processing. principal component analysis is applied on the formulated 13 dimensional feature vector, the process of which is dealt in the next sub-section.

The new feature set formed from this step is considered for further investigation. The clustering and classification procedures are applied in succession to this feature vector for retinal vessel segmentation. During clustering and classification, the retinal vessel segmentation is viewed as a binary problem where a pixel can belong to a 'vessel' class or a 'non-vessel' class. These procedures are explained in the further sub-sections.

3.2.2.3. Clustering. The feature vector formulated through application of principal component analysis is given as input to the clustering algorithm. Clustering [41] is an unsupervised data mining technique that groups data based on a similarity measure. The blood vessel segmentation problem constitutes only two groups namely 'vessel' and 'non-vessel'. Hence the number of clusters to be formed is assigned to two. Among the clustering algorithms, K-means algorithm [42] is found to outperform in view of differentiating vessels and non-vessels. Manhattan's distance is used for grouping of clusters. The K-means algorithm applied for retinal vessel segmentation is presented in Procedure 5.

- Step 1: Randomly choose ($k=2$) instances from Dataset D (containing N instances) as the initial cluster centers
- Step 2: Assign each instance to the cluster to which it is most similar as follows:
 - Step 2a: For $i=1$ to N do

$$\text{clusterlabel}(i) = \min(\text{dist}(x_i, c_j))$$

$$\text{where ,}$$

$$j = 1, 2 \text{ (number of clusters)}$$

$$x_i \text{ is the } i^{\text{th}} \text{ instance from the dataset}$$

$$\text{dist}(x_i, c_j) = \text{Manhattan distance between two instances}$$

$$\text{calculated as } |x_{i_1} - c_{j_1}| + \dots + |x_{i_m} - c_{j_m}|$$

$$m \text{ is the number of attributes (13 in this case)}$$
- Step 3: Update the cluster means
 - For all $j=1,2$

$$\text{average}_j = \text{Mean}(x_i \text{ whose clusterlabel}(i) = j)$$
- Step 3: For all $j=1,2$

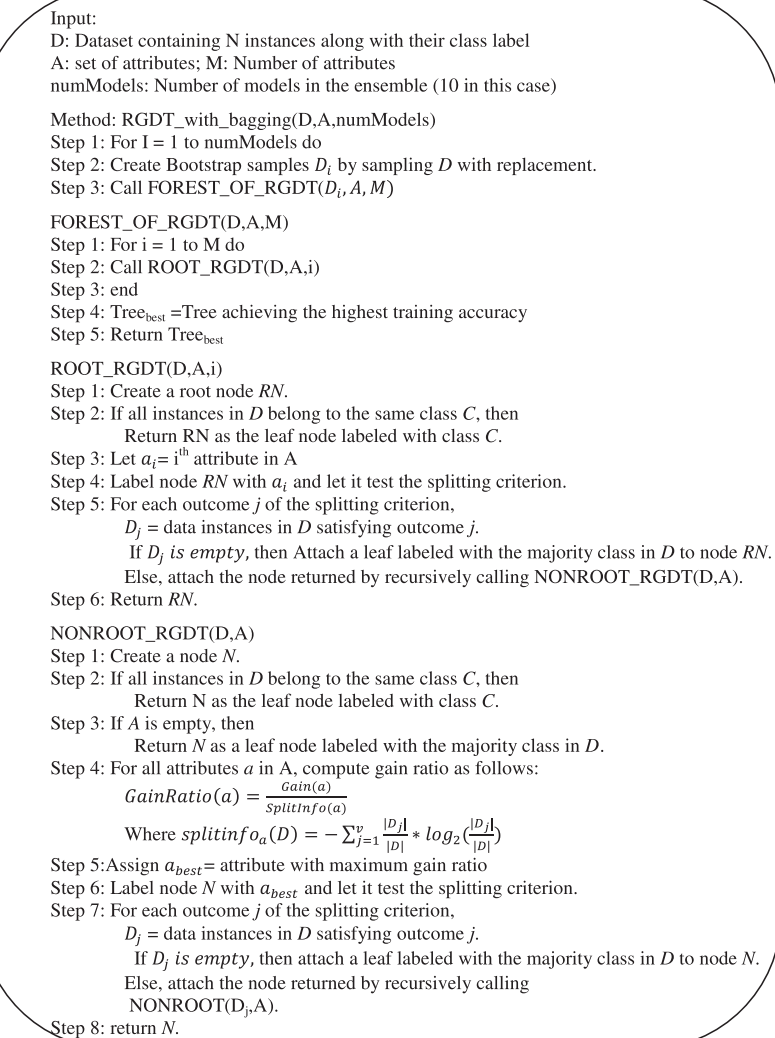
$$\text{prevAverage}_j = \text{average}_j$$
- Step 4: Iterate steps 2 and 3 until there is no change between prevAverage_j and average_j .

Procedure 5: K-means algorithm for retinal vessel segmentation.

As a result of the clustering algorithm, two clusters of uneven size are obtained. The size of the two clusters varies drastically such that approximately 10% of the data are grouped into one cluster while the remaining 90% are grouped into the other cluster. This is in agreement with the distribution of the vessels and non-vessels in the fundus image where the vessels occupy approximately 10% of the pixels and the remaining are considered as non-vessel pixels. Hence the cluster with higher cardinality is considered as the cluster containing non-vessel pixels and the cluster with lesser cardinality is taken to be the cluster consisting of the vessel pixels. The pixels in the vessel cluster are finalized as vessel pixels. The cluster containing the non-vessel pixels are further processed to recognize the vessel pixels that may be present in it through supervised classification algorithm which is discussed in the next sub-section.

3.2.2.4. Ensemble classification. The 'non-vessel' cluster is further examined to spot the vessel pixels that may be wrongly clustered into the 'non-vessel' cluster. Supervised classification technique [43–45] is applied to this data for this purpose. Supervised classification technique places necessity of training data as a pre-requisite. One of the images from the training set of

the database is given as training data. The ground truth of the corresponding image forms the label of the data. The classification technique derives decision rules from the training data. These decision rules can be used to classify the pixel data in the 'non-vessel' cluster to either a 'vessel' class or a 'non-vessel' class. Various classification algorithms were investigated, out of which root guided decision tree (RGDT) [46] performed the best. The root guided decision tree (RGDT) is a variant of decision tree whose construction is based on the following notion. A forest of decision trees are generated such that every attribute is placed at the root node of any one of the trees in the forest. Having constructed the root node, the rest of the tree construction is similar to that of the traditional decision tree construction. If there are m attributes in the data, m trees are generated in the forest. The tree which yielded the highest training accuracy is considered for deriving the classification rules. The performance of the classifier was still enhanced through the application of meta-learning algorithms, from which the bagging [47] could yield promising results. Thus the ensemble of RGDT through Bagging resulted in better pixel classification. The decision rules are obtained from the ensemble classification model in accordance with the algorithm depicted in *Procedure 6*.



Procedure 6: Algorithm for ensemble classification through RGDT with bagging.

Classification of the 'non-vessel' cluster would yield two classes namely 'vessel' class and 'non-vessel' class. In view of retinal blood vessel segmentation, the 'non-vessel' class resulted from the classification step is finalized as non-vessel pixels. The 'vessel' cluster from the clustering step and the 'vessel' class from the classification step combined together are concluded as vessel pixels. The result of clustering followed by classification would yield a binary vessel segmented image portraying the vessel as white and the non-vessel pixels as black. Sample segmentation results obtained from the unsupervised and supervised learning phase are shown in Fig. 7(a) and (b). This image can now be post-processed to yield at still cleaner and better segmentation. The details of the image post-processing phase are provided in the subsequent section.

3.2.3. Image post-processing phase

The previous phase outputs a binary vessel segmented image, which is further post-processed using mathematical morphology techniques [48] and connected component analysis. On examining the output image, it could be seen that the border of the field of view is also detected as vessels in a few images. This may be due to Gabor filtering, which actually enhances the high frequency components while the border of field of view also falls under high frequency category. Hence the mask of field of view is constructed and shrunk such that the radius is reduced by 25 pixels. It is superimposed on the output image to eliminate the unwanted arc like structures. Followed by the elimination of the arc, cleaning is performed to remove the isolated vessel pixels and spurs. Additionally, a majority

based procedure is performed where a pixel is set to vessel if 5 or more pixels in its 3 by 3 neighborhood are vessels. The resultant image still consisted of patch like structures occupying very less number of pixels (less than that occupied by the thin vessels). Hence the components which occupy less than 10 pixels are eradicated using connected component analysis. Finally a bridging operation is done which tries to connect the unconnected vessel pixels by assigning a pixel to vessel if it has two vessel neighbors that are not connected. The final outcome represents a clean and accurate segmentation of the retinal blood vessels. The data mining segmented image, post-processed segmented image and the corresponding ground truth of the sample fundus images are exhibited in Fig. 7(a) and (b). Thus the highlights of our work includes: the image pre-processing consists of image cropping to reduce the number of pixels would leads to lesser computational time; contrast enhancement to enhance the vessels; Gabor filtering, an extensively used directional filter for vessel enhancement was utilized to still enhance the vessels and halfwave rectification was performed to eliminate the noise due to Gabor filtering. Then combination of clustering and classification was attempted on feature vector obtained through application of principal component analysis on the preprocessed images in view to enhance the accuracy as they do not perform appreciably when used separately. The vessel and non-vessel cluster was considered for further processing to increase the performance of vessel segmentation. Classification was done on these clusters separately. It was observed that the further classification on vessel cluster increased the accuracy but decreased the sensitivity measure in some cases

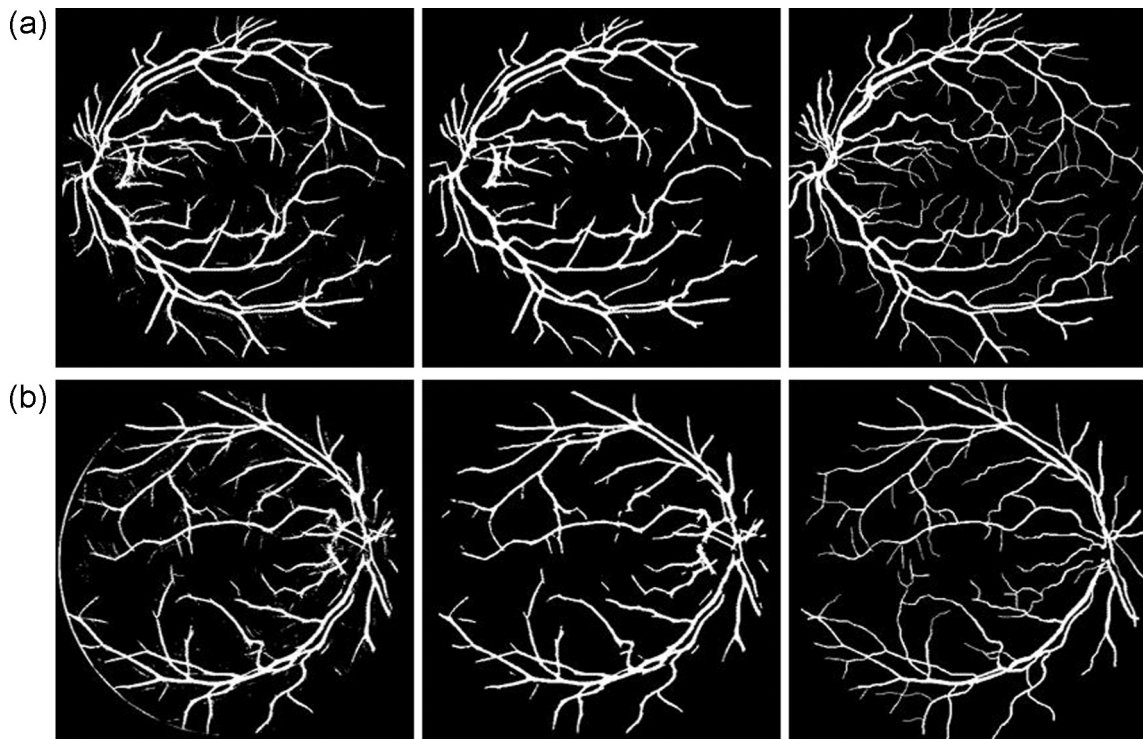


Fig. 7 – (a) Segmented outcome of data mining phase, post-processing phase and the corresponding ground truth of the first sample image (left eye image). **(b)** Segmented outcome of data mining phase, post-processing phase and the corresponding ground truth of the second sample image (right eye image).

while classification on the non-vessel cluster resulted in both higher accuracy and higher sensitivity when compared to the results of the clustering. Always, ensemble classification provided better results than individual classification. Hence, ensemble classification was adopted. Since the data mining algorithms do not consider the connectivity of the pixels which is an inherent property of the vessel structure, mathematical morphological techniques are applied for this purpose. Hence the proposed methodology is expected to achieve comparable performances when compared with existing techniques.

The results and discussions of the proposed framework in segmenting the retinal blood vessels from the fundus images are highlighted in next section.

4. Results and discussion

In this work, computational approaches are applied to segment the retinal blood vessels from the fundus image and segmentation accuracy is found to be better than the existing methodologies. The proposed framework is validated on the test images from the DRIVE [6,35] database. The proposed technique can assist the ophthalmologists in better retinal image analysis. The segmentation of blood vessels from fundus images can help in diagnosing the retinal disorders at an earlier stage and thus aid in better fruitful treatment to the patients.

The proposed system is implemented using Matlab r2008a and Weka 3.6.11 on a PC with i5 processor at 2.53 GHz and 4 GB RAM. The image pre-processing and post-processing phases were implemented through Matlab r2008a and unsupervised and supervised learning phase was executed using Weka 3.6.11, an open source data mining tool. It takes around 20 min for segmentation of a retinal fundus image (17 min for executing the procedures of image pre-processing phase; 2 min for executing the supervised and unsupervised learning phase and 45 s for the execution of image post-processing phase). It is to be noted that it consumes approximately 2 and a half hours for initial training of the data mining ensemble classifier. CPU usage reaches up to 55% with memory usage of 1.65 GB during image pre-processing while CPU usage of 35% and memory usage of 3.05 GB is consumed during execution of the unsupervised and supervised learning phase.

The RGB images were used for experimentation. Image enhancement techniques were employed to improve the contrast of the blood vessels on the retinal images so that it would be easier for segmentation. Green channel showed the highest contrast among the three channels of the RGB color model. When proceeded with the green channel and its Gabor responses, impressive accuracies could not be achieved. Hence, color space transformation was performed and the color channels (G , Y , L , $G1$) which exhibited the maximum contrast in each color model was chosen. Contrast limited adaptive histogram equalization (CLAHE) was applied to these images so that the contrast was still increased. Unlike other contrast enhancement methods, CLAHE limits the contrast and thus avoids over emphasizing the noise present in the image. Following the application of contrast enhancement on the images, Initially a feature vector constituting the intensities of these contrast enhanced images was formed and attempted for classification of vessel and non-vessel pixels, but could not

achieve appreciable accuracies. Hence the necessity of more features was realized. Gabor filtering is the most commonly used technique to enhance the blood vessels hence Gabor responses of the four color channel images were obtained. The performance of the Gabor filter greatly depends on its parameters. Hence various parameter settings were tried and the parameters which yielded the best visual results are reported here. Gabor responses were affected by unwanted noise which is interpreted as false vessels. This noise in the output image from the Gabor responses was eliminated through Halfwave rectification. Again the threshold for halfwave rectification is chosen based on various experiments. Threshold value of 10 yielded best subjective results. At this stage we have three Gabor responses for each of the four contrast enhanced images. During experiments it was seen that the results of segmentation with only Gabor responses as the feature vector, accuracies were comparable but the sensitivity dropped drastically. Hence, experiments were performed by including Green channel along with the 12 Gabor responses to find the accuracy and the sensitivity reaching comparable levels. Thus, the final feature vector was a 13D vector with the intensities of contrast enhanced Green channel and all the halfwave rectified Gabor responses.

Subsequently during the unsupervised and supervised learning phase, various combinations of techniques were attempted. Initially clustering and classification was performed individually. Both, when performed separately, reached higher accuracy rate but very low sensitivity measure (around 50–60%). In clustering, K-means attained the best partitioning. Hence it was again attempted with different distance measures and Manhattan distance was found to attain the best possible results. This process results in two unequal clusters, one with very high cardinality and the other with very low cardinality. The one with very high cardinality correspond to the non-vessel cluster while the one with very low cardinality pertain to the vessel cluster.

The vessel and non-vessel cluster was considered for further processing to increase the performance of vessel segmentation. Classification was done on these clusters separately. It was observed that further classification on vessel cluster increased the accuracy, but decreased the sensitivity measure in some cases, while classification on the non-vessel cluster resulted in both higher accuracy and higher sensitivity when compared to the results of the K-means clustering. Different classifiers were used for the purpose of vessel and non-vessel prediction. Initially C4.5 performed the best achieving an accuracy of 95.15%. Then a variation of decision tree, root guided decision tree (RGDT) was suggested which yielded the still higher accuracy and sensitivity.

Usually, the performance of the classifiers is enhanced through ensemble methods. In this case, Bagging resulted in high accuracies. The predictions obtained from clustering and ensemble classification are combined to form the segmented image, which is post-processed with basic mathematical morphology techniques to yield better segmented output. The experimental result of each image of the database and the method of computation of the metrics is discussed in the following paragraphs.

The performance of the proposed methodology on segmenting vessels from a fundus image is computed with the ground

truth of the corresponding image as reference. To quantify the performance of the proposed research work, performance metrics namely accuracy, sensitivity, specificity and positive predictive value were calculated. This evaluation scheme portrays the efficiency of the proposed framework in segmenting the retinal blood vessels of the fundus image. Four measures i.e., true positives, false positives, false negatives and true negatives have to be determined for the computation of the above mentioned performance metrics. True positive (TP) denotes the number of vessel pixels being correctly identified as vessels and true negative (TN) signifies the number of non-vessel pixels being correctly detected as non-vessels whereas false positive (FP) represents the number of non-vessels being wrongly classified as vessels and the false negative (FN) corresponds to the number of vessel pixels wrongly recognized as non-vessels. Using the values of TP, TN, FP and FN, the performance metrics, accuracy, sensitivity, specificity [49,50] and positive predictive value [3] is computed as follows.

Accuracy, defined as the ratio of sum of correctly identified vessels and non-vessels to the sum of total number of pixels, is calculated as shown in Eq. (3).

$$\text{Accuracy} = \frac{TP + TN}{TP + FP + FN + TN} \quad (3)$$

Sensitivity, defined as the ratio of correctly identified vessels to the total number of vessels, is computed as given in Eq. (4).

$$\text{Sensitivity} = \frac{TP}{TP + FN} \quad (4)$$

Specificity, defined as the ratio of correctly detected non-vessels to the total number of non-vessels, is measured as depicted in Eq. (5).

$$\text{Specificity} = \frac{TN}{TN + FP} \quad (5)$$

Positive predictive value [3] reveals the probability of a pixel that has been classified as a vessel is really a vessel as portrayed in Eq. (6).

$$\text{Positive Predictive Value} = \frac{TP}{TP + FP} \quad (6)$$

The performance of the proposed framework is demonstrated in Table 1. Table 1 tabulates the accuracy, sensitivity, specificity and positive predictive value of all images in the test set of DRIVE database. The average accuracy, sensitivity, specificity and positive prediction value is accomplished by the proposed approach is 95.36%, 70.79%, 97.78% and 75.76% respectively. The accuracy, sensitivity and specificity of segmentation in diseased images compute to 94.70%, 74.08% and 96.65%. The mean accuracy, sensitivity and specificity of vessel segmentation performance in normal images are 95.52%, 69.97% and 98.06%.

A comparison with the existing methodologies is presented in Table 2. Table 2 reveals the accuracy, sensitivity and

Table 2 – Performance comparison with the existing methodologies.

Technique	Accuracy (%)	Sensitivity (%)	Specificity (%)
Proposed technique	95.36	70.79	97.78
Second observer	94.70	77.96	97.17
Franklin et al. [3]	95.03	68.67	98.24
Lam et al. [33]	94.72	–	–
Akram et al. [24]	94.69	–	–
Soares et al. [7]	94.66	–	–
Miri and Mahloojifar [21]	94.58	73.52	97.95
Mendonca and Campilho [20]	94.52	73.44	97.64
Marin et al. [8]	94.52	70.67	98.01
Staal et al. [5]	94.41	–	–
You et al. [10]	94.34	74.10	97.51
Fraz et al. [22]	94.30	71.52	97.69
Anzalone et al. [27]	94.19	–	–
Niemeijer et al. [6]	94.16	–	–
Yanli Hou [31]	94.15	73.54	96.91
Saffarzadeh et al. [29]	93.87	–	–
Zhang et al. [15]	93.82	71.20	97.24
Bankhead et al. [23]	93.71	70.27	97.17
Chakrabortu et al. [19]	93.70	–	–
Espona et al. [34]	93.52	74.36	96.15
Martinez Perez et al. [26]	93.44	72.46	96.55
Xu et al. [9]	93.28	77.60	–
Cinsdikici and Aydin [14]	92.93	–	–
Vlachos and Dermatas [28]	92.90	74.70	95.50
Xiaoyi and Mojon [13]	92.12	–	–
Martinez Perez et al. [25]	91.81	63.89	–
Kande et al. [12]	89.11	–	–
Chauduri et al. [11]	87.73	–	–

Table 1 – Performance of the proposed methodology.

Image ID	Accuracy (%)	Sensitivity (%)	Specificity (%)	Positive predictive value (%)
01_test	95.20	74.31	97.24	72.52
02_test	95.92	71.03	98.76	86.69
03_test	94.45	73.53	96.77	71.57
04_test	95.61	68.60	98.34	80.78
05_test	95.48	71.70	97.93	78.24
06_test	95.25	61.67	98.87	85.43
07_test	95.40	69.02	98.10	78.09
08_test	94.98	66.33	97.68	75.18
09_test	95.77	61.92	98.76	81.47
10_test	95.66	73.90	97.61	73.51
11_test	94.71	68.62	97.28	71.27
12_test	95.46	73.76	97.48	73.94
13_test	95.11	65.13	98.36	81.10
14_test	95.53	73.62	97.45	71.81
15_test	93.84	82.82	94.68	54.59
16_test	95.78	66.12	98.72	83.66
17_test	95.66	62.31	98.72	80.81
18_test	95.90	72.22	97.94	75.12
19_test	95.49	81.40	97.55	69.47
20_test	95.92	77.85	97.35	70.02
Average	95.36	70.79	97.78	75.76

specificity obtained through various existing segmentation approaches on the DRIVE data. Hence from **Table 2**, it is obvious that the proposed algorithm achieves comparable results with the existing methodologies. From the extensive survey of blood vessel segmentation methodologies, it is also seen that an increase of 0.03% in accuracy is also considered significant in the segmentation of retinal blood vessels as it can aid in better disease diagnosis during further processing. Additionally, the number of pixels in the image is very high (329,960). Hence an increase of 0.33% (achieved by our algorithm) corresponds to around increased 1089 correctly predicted pixels.

Hence it is exhibited that the proposed work has accurately segmented the blood vessels from the retinal fundus images. The segmented vessels have to be further investigated for the purpose of disease diagnosis. Particularly, diabetic retinopathy, artery and vein occlusion, hypertensive retinopathy can be diagnosed from the segmented vessel tree. Thus the framework can aid the ophthalmologists in screening of retinal disorders more efficiently.

5. Conclusion

In this paper, solution to the problem of blood vessel segmentation is attempted through the utilization of computational intelligence. The proposed framework consists of image pre-processing phase, unsupervised and supervised learning phase and image post-processing phase where each phase includes its own set of procedures to be executed. The advantages of various techniques have been collectively utilized to achieve better performance. The performance of the proposed system is validated on test images of publicly available DRIVE database. It is seen that the proposed methodology achieves higher accuracy in vessel segmentation when compared to the existing techniques. Our methodology achieves an average accuracy, sensitivity and specificity of 95.36%, 70.79% and 97.78%. The demonstrated effectiveness of the proposed technique can thus help the ophthalmologists in efficient retinal image analysis and fruitful treatment to the patient community. The future insights include designing a new clustering algorithm that can group or classify the image pixels to vessel or non-vessels more precisely. Enhanced post-processing techniques can also be applied for better results.

Acknowledgement

This work was supported by Anna University under the UGC-BSR fellowship scheme, India (Reference: 27-DIST/UGC-BSR Res. Fellowship/2013-5).

REFERENCES

- [1] Abràmoff MD, Garvin MK, Sonka M. Retinal imaging and image analysis. *IEEE Trans Med Imaging* 2010;1(3): 169–208.
- [2] Patton N, et al. Retinal image analysis: concepts, applications and potential. *Prog Retin Eye Res* 2006;25:99–127.
- [3] Franklin SW, Rajan SE. Computerized screening of diabetic retinopathy employing blood vessel segmentation in retinal images. *Biocybern Biomed Eng* 2014;34:117–24.
- [4] Fraz MM, Remagnino P, Hoppe A, et al. Blood vessel segmentation methodologies in retinal images – a survey. *Comput Methods Programs Biomed* 2012;108(1):407–33.
- [5] Staal J, Abramoff MD, Niemeijer M, et al. Ridge-based vessel segmentation in color images of the retina. *IEEE Trans Med Imaging* 2004;23:501–9.
- [6] Niemeijer MJJ, Staal B, van Ginneken. et al. Comparative study on retinal vessel segmentation methods on a new publicly available database. *SPIE* 2004;648–56.
- [7] Soares JVB, Leandro J.J.G., Cesar RM, et al. Retinal vessel segmentation using the 2-D Gabor wavelet and supervised classification. *IEEE Trans Med Imaging* 2006;25:1214–22.
- [8] Marin D, Aquino A, Gegundez-Arias ME, Bravo JM. A new supervised method for blood vessel segmentation in retinal images by using gray-level and moments invariants-based features. *IEEE Trans Med Imaging* 2011;30(1):146–58.
- [9] Xu L, Luo S. A novel method for blood vessel detection from retinal images. *BioMed Eng Online* 2010;9(14).
- [10] You X, Peng Q, Yuan Y, et al. Segmentation of retinal blood vessels using the radial projection and semi-supervised approach. *Pattern Recognit* 2011;44:2314–24.
- [11] Chaudhuri S, Chatterjee S, Katz N, et al. Detection of blood vessels in retinal images using two-dimensional matched filters. *IEEE Trans Med Imaging* 1989;8:263–9.
- [12] Kande GB, Subbaiah PV, Savithri TS. Unsupervised fuzzy based vessel segmentation in pathological digital fundus images. *J Med Syst* 2009;34:849–58.
- [13] Xiaoyi J, Mojón D. Adaptive local thresholding by verification-based multithreshold probing with application to vessel detection in retinal images. *IEEE Trans Pattern Anal Mach Intell* 2003;25:131–7.
- [14] Cinsdikici MG, Aydin D. Detection of blood vessels in ophthalmoscope images using MF/ant (matched filter/ant colony) algorithm. *Comput Methods Programs Biomed* 2009;96:85–95.
- [15] Zhang B, Zhang L, Zhang L, Karray F. Retinal vessel extraction by matched filter with first-order derivative of Gaussian. *Comput Biol Med* 2010;40:438–45.
- [16] Frangi A, Niessen W, Vincken K, Viergever M. Multiscale vessel enhancement filtering. *Proc Med Image Comput* 1998;1496:130–7.
- [17] Budai A, Bock R, Maler A, et al. Robust vessel segmentation in fundus image. *Int J BioMed Imaging* 2013;1–11.
- [18] Hannink J, Dutta R, Bekkers E. Crossing-preserving multiscale vesselness. *Medical image computing and computer-assisted intervention. Lect Notes Comput Sci* 2014;8674:603–10.
- [19] Chakraborti T, Chowdry AS. A Self-Adaptive Matched Filter for Retinal Blood Vessel Detection. *Machine Vision and Applications*. Berlin HeidelBerg: Springer Verlag; 2014.
- [20] Mendonça AM, Campilho A. Segmentation of retinal blood vessels by combining the detection of centerlines and morphological reconstruction. *IEEE Trans Med Imaging* 2006;25:1200–13.
- [21] Miri MS, Mahloojifar A. Retinal image analysis using curvelet transform and multistructural elements morphology by reconstruction. *IEEE Trans Biomed Eng* 2011;58:1183–92.
- [22] Fraz MM, Barman SA, Remagnino P, et al. An approach to localize the retinal blood vessels using bit planes and centerline detection. *Comput Methods Programs Biomed* 2012;108(2):600–16.

- [23] Bankhead P, Scholfield CN, McGeown JG, Curtis TM. Fast retinal vessel detection and measurement using wavelets and edge location refinement. *PLoS ONE* 2012;7(3):e32435.
- [24] Usman Akram M, Khan SA. Multilayered thresholding-based blood vessel segmentation for screening of diabetic retinopathy. *Eng Comput* 2013;29(2):165–73.
- [25] Martinez-Perez ME, Hughes AD, Stanton AV, et al. Retinal blood vessel segmentation by means of scale-space analysis and region growing. The Second International Conference on Medical Image Computing and Computer-Assisted Intervention. London, UK: Springer-Verlag; 1999. p. 90–7.
- [26] Martinez-Perez ME, Hughes AD, Thom SA, et al. Segmentation of blood vessels from red-free and fluorescein retinal images. *Med Image Anal* 2007;11:47–61.
- [27] Anzalone A, Bizzarri F, Parodi M, Storace M. A modular supervised algorithm for vessel segmentation in red-free retinal images. *Comput Biol Med* 2008;38:913–22.
- [28] Vlachos M, Dermatas E. Multi-scale retinal vessel segmentation using line tracking. *Comput Med Imaging Graph* 2009;34:213–27.
- [29] Saffarzadeh VM, Osareh A, Shadgar B. Vessel segmentation in retinal images using multi-scale line operator and K-means clustering. *J Med Signals Sens* 2014;4(2):122–9.
- [30] Zhou L, Rzeszotarski MS, Singerman LJ, Chokreff JM. The detection and quantification of retinopathy using digital angiograms. *IEEE Trans Med Imaging* 1994;13(4):619–26.
- [31] Can A, Shen H, Turner JN, et al. Rapid automated tracing and feature extraction from retinal fundus images using direct exploratory algorithms. *IEEE Trans Inf Technol Biomed* 1999;3(2):125–38.
- [32] Tolias Y, Panas SM. A fuzzy vessel tracking algorithm for retinal images based on fuzzy clustering. *IEEE Trans Med Imaging* 1998;17(2):263–73.
- [33] Lam BSY, Yongsheng G, Liew AWC. General retinal vessel segmentation using regularization-based multiconcavity modeling. *IEEE Trans Med Imaging* 2010;29:1369–81.
- [34] Espona L, Carreira MJ, Penedo MG, Ortega M. Retinal vessel tree segmentation using a deformable contour model. ICPR, 19th International Conference on Pattern Recognition. 2008. pp. 1–4.
- [35] Niemeijer M, Staal JJ, Ginneken Bv, Loog M, Abramoff MD. DRIVE: Digital Retinal Images for Vessel Extraction; 2004, <http://www.isi.uu.nl/Research/Databases/DRIVE>.
- [36] Brainard DH. Calibration of computer controlled color monitor. *Color Res Appl* 1989;14(1):23–34.
- [37] Geusebroek J, et al. Color invariance. *IEEE Trans Pattern Anal Mach Intell* 2001;23(2):1338–50.
- [38] Pizer SM, Philipi Amburn E, Austin JD, et al. Adaptive histogram equalization and its variations. *Comput Vis Graph Image Process* 1987;39:355–68.
- [39] Fogel I, Sagi D. Gabor filters as texture discriminator. *Biol Cybern* 1989;61(2).
- [40] Jolliffe IT. Principal Component Analysis. ISBN 978-0-387-95442-4 Springer-Verlag; 1986. p. 487.
- [41] Nancy P, Geetha Ramani R. Discovery of patterns and evaluation of clustering algorithms in social network data (Facebook 100 universities) through data mining methods and techniques. *Int J Data Min Knowl Manag Process (IJDKP)* 2012;2(5).
- [42] Lloyd SP. Least squares quantization in PCM. *IEEE Trans Inf Theory* 1982;28:128–37.
- [43] Geetha Ramani R, Jacob SG. Prediction of P53 mutants (multiple sites) transcriptional activity based on structural (2D&3D) properties. *PLOS ONE* 2013;8(2):e55401.
- [44] Geetha Ramani R, Balasubramanian L. Multi-class classification for prediction of retinal diseases (retinopathy and occlusion) from fundus images. ICKM. 2013. pp. 122–34.
- [45] Geetha Ramani R, Balasubramanian L, Jacob SG. ROC analysis of classifiers in automatic detection of diabetic retinopathy using shape features of fundus images. International Conference on Advances in Computing, Communications and Informatics. 2013. pp. 66–72.
- [46] Geetha Ramani R, Balasubramanian L, Alaghu Meenal A. Decision tree variants (absolute random decision tree and root guided decision tree) for improved classification of data. *Int J Appl Eng Res* 2015;10(17):13190–5.
- [47] Breiman L. Bagging predictors. *Mach Learn* 1996;24(2):123–40.
- [48] Gonzalez RC. Digital Image Processing. 3rd ed. Prentice Hall; 2008.
- [49] Geetha Ramani R, Balasubramanian L, Jacob SG. Automatic prediction of diabetic retinopathy and glaucoma through image processing and data mining techniques. International Conference on Machine Vision and Image Processing. 2012. pp. 163–7.
- [50] Geetha Ramani R, Balasubramanian L, Jacob SG. Data mining method of evaluating classifier prediction accuracy in retinal data. IEEE International Conference on Computational Intelligence and Computing Research. 2012. pp. 426–9.